Pflugers Arch - Eur J Physiol (2017) 469:797–813
DOI 10.1007/s00424-016-1930-6

SIGNALING AND CELL PHYSIOLOGY

Interstitial cell modulation of pyeloureteric peristalsis in the mouse renal pelvis examined using FIBSEM tomography and calcium indicators

Hikaru Hashitani[1] · Michael J. Nguyen[2] · Haruka Noda[1] · Retsu Mitsui[1] · Ryuhei Higashi[3] · Keisuke Ohta[3] · Kei-Ichiro Nakamura[3] · Richard J. Lang[2]

Received: 30 November 2016 / Accepted: 12 December 2016 / Published online: 4 January 2017

Abstract Typical and atypical smooth muscle cells (TSMCs and ASMCs, respectively) and interstitial cells (ICs) within the pacemaker region of the mouse renal pelvis were examined using focused ion beam scanning electron (FIB SEM) tomography, immunohistochemistry and Ca^{2+} imaging. Individual cells within 500–900 electron micrograph stacks were volume rendered and associations with their neighbours established. 'Ribbon-shaped', Ano1 Cl^- channel immunoreactive ICs were present in the adventitia and the suburothelial space adjacent to the TSMC layer. ICs in the proximal renal pelvis were immuno-reactive to antibodies for $Ca_V3.1$ and hyperpolarization-activated cation nucleotide-gated isoform 3 (HCN3) channel sub-units, while basal-epithelial cells (BECs) were intensely immuno-reactive to Kv7.5 channel antibodies. Adventitial to the TSMC layer, ASMCs formed close appositions with TSMCs and ICs. The T-type Ca^{2+}channel blocker, Ni^{2+} (10–200 μM), reduced the frequency while the L-type Ca^{2+} channel blocker (1 μM nifedipine) reduced the amplitude of propagating Ca^{2+} waves and contractions in the TSMC layer. Upon complete suppression of Ca^{2+} entry through TSMC Ca^{2+} channels, ASMCs displayed high-frequency (6 min^{-1}) Ca^{2+} transients, and ICs distributed into two populations of cells firing at 1 and 3 min^{-1}, respectively. IC Ca^{2+} transients periodically (every 3–5 min^{-1}) summed into bursts which doubled the frequency of ASMC Ca^{2+} transient firing. Synchronized IC bursting and the acceleration of ASMC firing were inhibited upon blockade of HCN channels with ZD7288 or cell-to-cell coupling with carbenoxolone. While ASMCs appear to be the primary pacemaker driving pyeloureteric peristalsis, it was concluded that sub-urothelial HCN3(+), $Ca_V3.1$(+) ICs can accelerate ASMC Ca^{2+} signalling.

Keywords Pyeloureteric peristalsis · Upper urinary tract · Focused ion bean scanning electron microscopy · Calcium · Smooth muscle cells

Abbreviations

α-SMA	α-Smooth muscle actin
Ano1	Antoctamin-1 Ca^{2+}-activated Cl^- channel encoded by the ANO1 gene
ASMC	Atypical smooth muscle cell
BEC	Basal epithelial cell
BK channel	Large conductance calcium-activated potassium channel
$[Ca^{2+}]_i$	Intracellular concentration of Ca^{2+}
Cap	Capillary
$Ca_V3.x$	'T-type' Ca^{2+} channel
CIRC	Ca^{2+}-induced release of Ca^{2+}
DAPI	4′,6-Diamidino-2-phenylindole dihydrochloride
DMSO	Dimethyl sulphoxide
eYFP	Enhanced-yellow fluorescent protein
FIB SEM	Focused ion bean scanning electron microscopy
F_t/F_0	Ratio (F_t/F_0) of the fluorescence at time t and baseline fluorescence at $t = 0$
GFP	Green fluorescent protein

Electronic supplementary material The online version of this article (doi:10.1007/s00424-016-1930-6) contains supplementary material, which is available to authorized users.

✉ Richard J. Lang
rick.lang@monash.edu

[1] Department of Cell Physiology, Nagoya City University Graduate School of Medical Sciences, Nagoya 467-8601, Japan

[2] Department of Pharmacology, School of Biomedical Sciences, Monash University, Clayton, VIC 3800, Australia

[3] Department of Anatomy, Kurume University School of Medicine, Kurume, Japan

K_{ATP}	Glibenclamide-sensitive ATP-dependent K^+ channels
$K_V7.x$	K channel subunit encoded by KCNQx gene
HCN	Hyperpolarization-activated cation nucleotide-gated channel
ICs	Interstitial cells
ICC	Interstitial cells of Cajal
IP_3	Inositol triphosphate
MAS	An original glass slide product of Matsunami Glass, Osaka, Japan. http://www.matsunami-glass.co.jp/english/life/clinical_g/data18.html
MASSIVE	Multi-modal Australian ScienceS Imaging and Visualisation Environment
N	Number of animals
n	Number of cells
NB	Nerve bundle
OCT	Optimal cutting temperature
P	Papilla
PBS	Phosphate-buffered saline
PDGFRα	Platelet-derived growth factor receptor alpha
PG	Prostaglandin
PSS	Physiological salt solution
RA	Renal artery
RIC	Renal interstitial cell
RV	Renal vein
ROI	Region of interest
STDs	Spontaneous transient depolarizations
TSMC	Typical smooth muscle cell
U	Urothelium
½ width	Half-amplitude duration measured as the time between 50% peak amplitudes on the rising and falling phases

Introduction

Despite the essential role pyeloureteric peristalsis plays in sustaining the homeostatic functions of the kidney, the nature of the intrinsic pacemaker mechanisms driving this movement of urine and water-soluble toxic waste towards the bladder has yet to be unequivocally characterized. Using standard electron microscopy, Gosling and Dixon examined the ultrastructure of uni-calyceal and multi-calyceal kidneys [7–9, 12] and proposed that the pacemaker cells driving the peristaltic contractions were morphologically distinct smooth muscle cells they called 'atypical' smooth muscle cells (ASMCs). In uni-calyceal kidneys, ASMCs are predominately located in the serosal surface of the renal pelvis wall as it approaches the base of the papilla [12].

In proximal regions of contraction-arrested renal pelvis preparations of the guinea pig, rat and mouse, spontaneous transient depolarisations (STDs) are readily recorded in ASMCS with intracellular microelectrodes [20, 23, 25, 28, 40], while spontaneous Ca^{2+} transients of similar frequency are recorded in ASMCs on the serosal surface of the typical smooth muscle cell (TSMC) layer of the mouse renal pelvis [25]. The discharge of both STDs and Ca^{2+} transients is exquisitely dependent on the uptake and release of Ca^{2+} from the endoplasmic reticulum and mitochondria [13, 26] suggesting that STDs are generated upon the flow of Ca^{2+}-activated inward currents triggered upon the spontaneous release of Ca^{2+} from ASMC internal stores [24]. In the absence of 'L-type' Ca^{2+} channel blockade, these STDs sum and trigger propagating action potentials which can be visualized as Ca^{2+} waves or contractions in the TSMC layer [25].

In this report, we aimed to establish the identity of the pacemaker cells driving pyeloureteric peristalsis, as well as the morphological relationships between TSMCs, ASMCs [12, 24] and ICs immuno-positive for hyperpolarization-activated cation nucleotide-gated isoform 3 (HCN3) channel sub-units [15]. Of particular interest was the examination of whether ICs can modulate the ASMC activity [20]. Using focused ion beam scanning electron microscopy (FIB SEM), the three-dimensional structure and spatial relationships between ICs, ASMCs and TSMCs within the pacemaker region of the mouse renal pelvis have been established. Cellular reconstructions involved the repeated milling (100 nm thick) of a block of proximal renal pelvis with the FIB, then SEM imaging the surface of each new face and volume rendering individual cells within the resulting stacks of ortho-slice micrographs. The nature of IC modulation of ASMC Ca^{2+} signalling was also elucidated using fluorescence imaging after the complete blockade of TSMC contractility. These IC-ASMC interactions were examined using blockers of hyperpolarization-activated cation nucleotide-gated (HCN) channels [15] or cell-to-cell coupling [25].

Material and methods

Conventional male or female (Balb/c and Amus Swiss) mice (3–8 weeks of age) were anaesthetized with isoflurane (4%) and killed by cervical dislocation and exsanguination. Kidneys were excised through an abdominal incision. All animal care and experimental protocols were in accordance with the National Health and Medical Research (Australia) guidelines and approved by the Animal Ethics Committees at Monash University, Kurume University School of Medicine and Nagoya City University Graduate School of Medicine.

Recording renal pelvic contraction

The renal pelvis attached to the parenchyma of bisected kidneys was dissected free of its surrounding fat and adventitia and pinned to the base of a recording chamber. The bath was then viewed with a dissection microscope and perfused (at

2 ml min^{-1}) with bicarbonate-buffered physiological salt solution (PSS see below) at 35 °C. Changes in the diameter at one point on the renal pelvis were recorded with a video camera and analysed with Diamtrak software. Pelvic diameter changes were often increased upon removal of the papilla [32, 33].

Focused ion beam scanning electron microscopy

Details of the fixation and processing of blocks of tissue and the use of beam deceleration and stage tilting with the FIB SEM have been previously described [35]. Briefly, mice were deeply anesthetized and transcardially perfused with heparin (10 U/ml)-containing saline followed by 2% paraformaldehyde, 2.5% glutaraldehyde and 2 mM $CaCl_2$ in 0.1 M cacodylate buffer (pH 7.4). The kidney was then removed and cut into blocks and further fixed for 2 h at room temperature. Blocks were then stained, embedded in resin, trimmed down to 1.5-mm^3 cubes using an Ultracut E microtome (Leica Germany) and mounted on a specimen holder for SEM imaging [35]. With a SEM (Quanta 3D FEG, FEI, Netherlands), the Y-Z surface of the block was first examined to locate the bulb region at the base of the septa attachments of the renal pelvis to the kidney parenchyma where both ASMCs and TSMCs are present in abundance.

A small area (100 × 100 μm^2) on the X-Y surface was then repeatedly trimmed (100 nm at a time) by ion beam milling using the FIB to reveal a new surface for imaging using the SEM (Fig. 1b). Three stacks of 500–900 images were captured on computer for later processing using a 3D visualization software (AVIZO 8.1, Visualization Sciences Group, FEI Comp.). Cell shapes were rendered using interpolations between every two to three slices within each image stack.

Immunohistochemistry

The methods describing the immuno-histochemical analysis using Ano1, HCN3 and $K_v7.5$ antibodies have been previously described [17]. For $Ca_V3.1$ and α-smooth muscle actin (α-SMA) immunostaining, the renal pelvis as well as attached kidney and ureter were immersed in optimal cutting temperature (OCT) compound (Sakura Finetek, Torrance, CA, USA) and frozen at −80 °C or the tissue was fixed with Zamboni's fixative for 2 h prior to the embedding in OCT compound. Sections (10 μm thick) were cut with a cryostat, mounted on MAS-coated glass slides (Matsunami Glass, Osaka, Japan) and dried. The sections for $Ca_V3.1$ staining were fixed in acetone for 15 min at 4 °C. Sections were incubated with phosphate-buffered saline (PBS) containing 0.3% Triton X-100 for 10 min, Block Ace for 20 min and then rabbit anti-$Ca_V3.1$ antibody (1:200, Alomone Labs, ACC-021) and/or mouse anti-α-SMA antibody (1:1000, clone 1A4, Sigma) for 4 days at 4 °C. After washing in PBS, sections were incubated with biotinylated swine anti-rabbit IgG antibody (1:300, Dako) for 30 min (only for $Ca_V3.1$ staining) and then incubated with Alexa488-conjugated streptavidin (10 μg ml^{-1}, Molecular Probes) and/or Cy3-conjugated goat anti-mouse IgG antibody (2.5 μg ml^{-1}, Chemicon) as well as the nuclei staining reagent Hoechst 33342 for 2 h. $Ca_V3.1$ immuno-reactivity detected in sections of mouse Purkinje cells was used as a positive control, supporting the specificity of this $Ca_V3.1$ antibody. Specimens were coverslipped and observed with a confocal laser scanning microscope (LSM 5 PASCAL, Zeiss).

Measurements of internal Ca^{2+} concentration

To visualize changes in the internal Ca^{2+} concentration ($[Ca^{2+}]_i$) in cells of the renal pelvis, preparations were pinned tightly, with their serosal surface uppermost, to the bottom of an organ bath and incubated with physiological salt solution (PSS 2 min^{-1} at 36 °C) until spontaneous muscle contractions appeared. Preparations were incubated in low-Ca^{2+} PSS ($[Ca^{2+}]_o$ = 0.1 mM) containing either 3 μM Cal-520AM (AAT Bioquest Inc.) or 1 μM Fluo-4AM (special packaging, Dojindo, Japan) and Cremophor EL (0.01%, Sigma) for 25–30 min at 35 °C, then 15–30 min at room temperature. Preparations were then superfused (2 min^{-1}) with dye-free, warmed PSS ($[Ca^{2+}]_o$ = 2.5 mM 36 °C). TSMCs were imaged at ×20 magnification, ICs and ASMCs at ×40 magnification, and all cells were sampled at 8–10 images per second.

Changes in $[Ca^{2+}]_i$ (Ca^{2+} transients) were expressed as the ratio (F_t/F_0) of the fluorescence generated at time t (F_t) and the baseline fluorescence at t = 0 (F_0) [17, 32].

Solutions and drugs used

The PSS had the following composition (mM): NaCl 120, KCl 5, $CaCl_2$ 2.5, $MgSO_4$ 2, KH_2PO_4 1, $NaHCO_3$ 25 and glucose 11, bubbled with a 95% O_2/5% CO_2 gas mixture to establish a pH of 7.3–7.4 in the bath. Indomethacin and nifedipine were dissolved in ethanol, and ZD7288 was dissolved in dimethyl sulphoxide (DMSO); neither vehicle exceeded a 1:1000 concentration.

Data analysis

The following parameters of the Ca^{2+} transients and contractions were measured: peak amplitude measured from the resting level; half-amplitude duration (½ width), measured as the time between 50% peak amplitudes on the rising and falling phases; and the area under each event (integral) and their frequency (min^{-1}) which was averaged over 2–3 min of recording. Variation of contraction

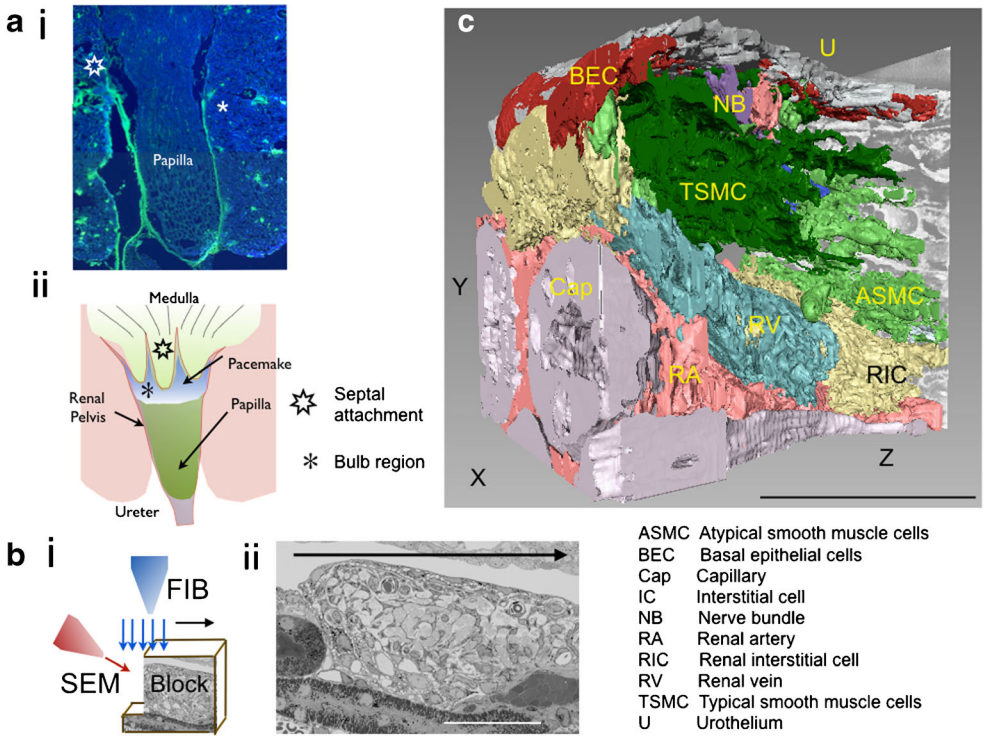

Fig. 1 The architecture of the mouse proximal renal pelvis examined using FIB SEM tomography. **a**, *i* Single caudal section illustrating that the mouse renal pelvis immuno-positive for anti-α-SMA antibodies (*green*) either becomes thinner as it approaches the papilla base (*star*) or ends abruptly as a 'bulb' (*asterisk*), thus forming a funnel-shaped structure, with a number of 'finger-like' septa attachments to the kidney parenchyma (**a**, *ii*). **b**, *i* Schematic of the focused ion beam scanning electron microscope (FIB SEM) in which the X-Y surface of a block of renal pelvis is repeatedly milled in the Z direction using the FIB, and each new X-Y surface is then imaged using the SEM. **b**, *ii* The Y-Z surface of the block of renal pelvis was first used to locate a bulb region of the renal pelvis for FIB SEM processing. **c** Similar-looking cells and structures within the block of 900 ortho-slice micrographs were identified and volume rendered by interpolation and colour coded for easy identification. Calibration *bars* 50 μm (**b**), 0.5e^5 nm (**c**) (colour figure online)

amplitudes was reduced by expressing the response in the presence of a drug (D) as a percentage change from control (C); i.e. $100 \times (D - C)\ C^{-1}$.

Data is presented as the mean ± standard error (SE) of the mean, with N denoting the number of tissues and n the number of cells. Paired or unpaired Student's t tests were used as tests of significance and corrected for multiple comparisons when necessary; $p < 0.05$ was accepted as statistically significant [17, 32].

Results

FIB SEM analysis of pelvis architecture

In most small mammals, the kidney contains a single pyramid-shaped renal medulla, which is surrounded by a single calyx or renal pelvis. This renal pelvis consists of a urothelium-lined lumen and a plexus of bundles of long TSMCs. Random longitudinal sections of the mouse kidney stained with anti-α-SMA reveal that the smooth muscle layer in the renal pelvis wall either becomes thinner as it approaches the papilla base or ends abruptly as a bulb (Fig. 1a(i)). These sections have been interpreted as the renal pelvis forming a funnel-shaped structure, with a number of 'finger-like' septa attachments to the kidney parenchyma (Fig. 1a(ii)).

The Y-Z surface of a renal pelvis block was first examined to locate a bulb region (Fig 1b(ii)). Once a bulb region was located, the X-Y surface of the block was repeatedly milled (100 nm slices) using the FIB to reveal a new surface that was imaged using the SEM (Fig. 1b(i)). The most proximal region of the bulb was first milled 900 times. Two additional image stacks of 500 and 700 ortho-slices were then obtained by the continued milling of the block in the Z direction (Supplementary Fig. 1a, bi–iii). Images within each stack were aligned, and similar-looking cells within the block were identified and volume rendered by interpolation between individual micrographs. Cells of similar morphology were colour coded for easy identification (Fig. 1c).

In the bulb region of the renal pelvis, the urothelium exists as a stratified squamous epithelium that consists of a thin layer of squamous epithelial cells lining the lumen and a layer of basal epithelial cells (BECs). The squamous epithelial cells formed a continuous layer of cells with long inter-connecting

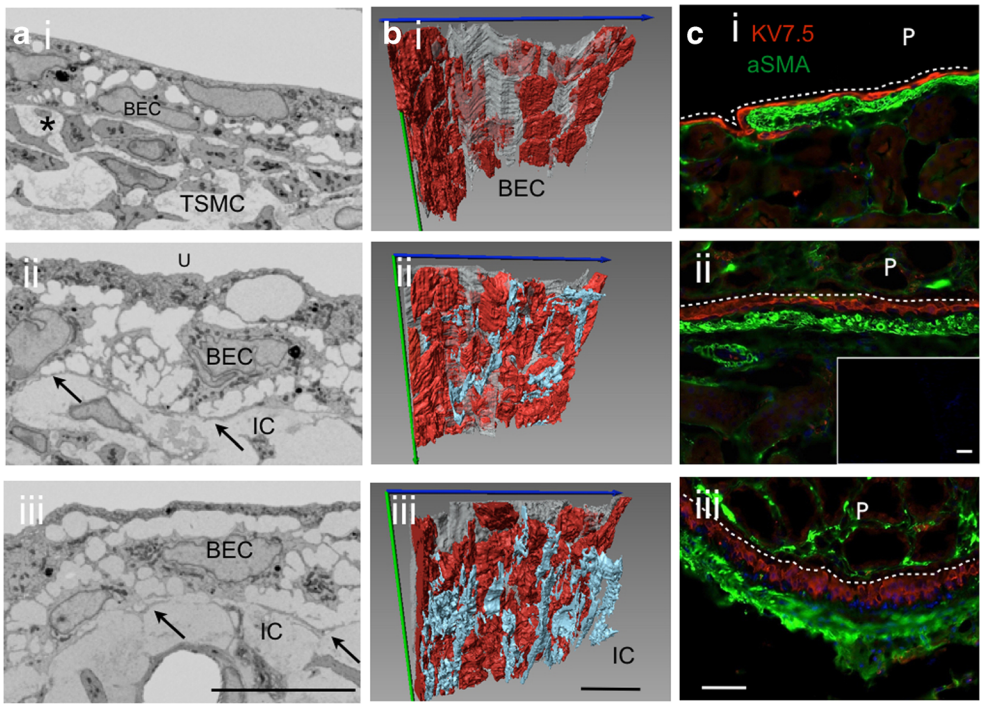

Fig. 2 Arrangement and associations of basal epithelial cells (BECs) and fibroblast-like interstitial cells (ICs) in the sub-urothelial space of the proximal renal pelvis. **a** BECs and ICs in the sub-urothelial space as seen using standard electron microscopy of the Y-Z surface of a block of the renal pelvis, to illustrate their close appositions with neighbouring cells. **b**, *i–iii* After volume rendering, ribbon-shaped sub-urothelial ICs (*pale blue cells*) have been displayed in the presence of volume-rendered BECs (**b**, *i–iii*, *red cells*), with all other cells removed. The urothelium (U) consists of a single continuous grey layer parallel to the Z axis. **c**, *i–iii* BECs are located in the same region as cells intensely immuno-reactive to antibodies against $K_V7.5$ channel sub-units. **c**, *ii inset*, a negative control. *P* represents the papilla, the *dashed line* represents the luminal surface of the urothelium. Calibration *bars* 10 μm (**a**), $0.2e^{14}$ nm (**b**, *i–iii*) and 50 μm (**c**, *ii–iii*) (colour figure online)

projections and a bugle at their nuclei (Fig. 2a(i–iii)) [6]. This urothelial layer (U) has been coloured grey and rendered as a single layer (Fig. 2b(i–iii)). BECs within the urothelial layer contained large round nuclei and numerous dense bodies, mitochondria and free ribosomes (Fig. 2 a(i–iii)), forming a single layer of loosely packed irregular-shaped cells with many short interconnecting cytoplasmic projections (Fig. 2a(i–iii)). When volume rendered, BECs (Fig 2b(i–iii) *red cells*) occupied the same morphological space as cells that are intensely immuno-reactive to antibodies raised against the $K_V7.5$ channel sub-unit (Fig. 2c(i–iii)). Both volume-rendered BECs (Fig. 2b(i–iii)) and $K_V7.5$(+) cells (Fig. 2c(i–iii)) increased in number and density with distance from the base of the papilla. At the point where the calyx no longer attaches to the renal substance, the urothelium abruptly changes into a tightly packed transitional epithelial layer, and both BECs and $K_V7.5$(+) cells increased in number so that the layer becomes three to five cells thick, presumably creating an impermeable barrier.

Sub-urothelial and serosal interstitial cells

'Fibroblast-like' ICs within the sub-urothelial space (Fig. 2a(ii–iii) *arrows*) and adventitia (Fig. 3a) have been previously described as 'ICC-like', being intensely immuno-positive for antibodies against the Ca^{2+}-activated Cl^- channel protein Ano1 and mildly immuno-positive for $K_V7.5$ antibodies [17, 34], as well as having a species-dependent expression for Kit [20, 29, 30]. Standard electron microscopic examination (Y-Z surface) within these two regions revealed the presence of sparsely distributed ICs (Figs. 2a(ii, iii) and 3a) separated by regions of dense bundles of collagen, the absence of any fibronexus indicating that these ICs were not myofibroblasts. There was no evidence of any ganglionic cell bodies.

In coronal sections of the whole renal pelvis, α-SMA(−)ICs immuno-reactive to antibodies against $Ca_V3.1$ ($Ca_V3.1$(+)) were selectively located within the sub-urothelial space, and no similar immuno-reactive product was observed in adventitial ICs (Fig. 4a, b(i, ii)). ICs in whole mount preparations of the proximal renal pelvis were also immuno-reactive to HCN3 antibodies (Fig. 4d(i, ii)). HCN3(+) cells in the mouse renal pelvis have been previously reported to be co-located with $Ca_V3.1$ channel immuno-reactivity [14] and present only in the proximal renal pelvis. In the present experiments, $Ca_V3.1$(+) ICs did not have the same distribution or morphology as PDGFRα(+) cells of B6.129S4-Pdgfr$\alpha^{tm11(EGFP)sor}$/J mice which are located on both sides of the muscularis, as well as the intermuscular space of the renal pelvis (Fig. 4c(i–iii)).

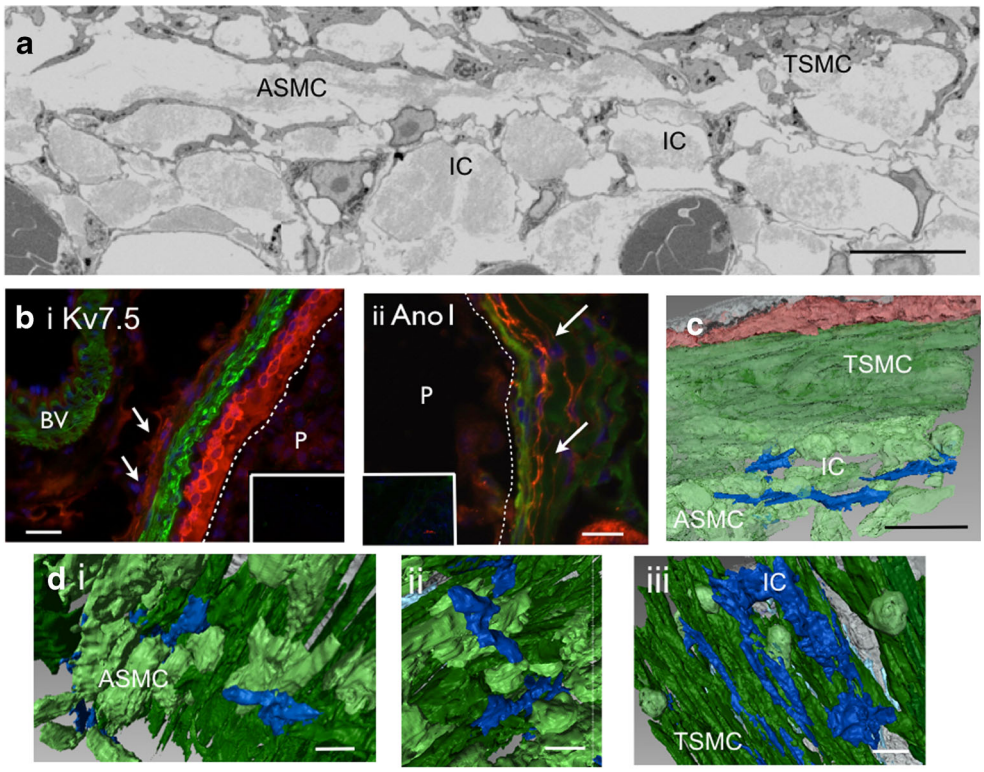

Fig. 3 **a** Standard electron micrograph of the serosal surface of the mouse proximal renal pelvis illustrating the structure and associations of ICs, ASMCs and TSMCs. **b** Superimposed micrographs of the renal pelvis stained with antibodies for $K_V7.5$ (*i*, *red*) or Ano1 (*ii*, *red*) and α-SMA (*i–ii*, green). *Insets* represent negative controls, *P* the papilla and the *dashed lines* the luminal surface. Micrographs of volume-rendered serosal ICs (*dark blue cells*), TSMCs (*dark green cells*) and ASMCs (*light green cells*) displayed at a low (**c**) and high (**d**, *i–iii*) magnification to illustrate their architecture and close appositions. Calibration *bars* 5 μm (**a**), 5 μm (**b**, *i–iii*), $2e^{13}$ nm (**c**, **d**) (colour figure online)

Standard electron microscopic examinations have suggested that fibroblast-like ICs in the sub-urothelium and adventitia increase in number with distance from the papilla base [20] suggesting that these $Ca_V3.1$(+) HCN3(+) ICs represent only a subset of the ICs present.

Volume rendering of ICs within the sub-urothelial space and adventitia revealed that they were in fact flat and 'ribbon shaped' (Figs. 2b(ii, iii) *pale blue cells*, and 3c, d *dark blue cells*), making close appositions with like cells, as well as neighbouring ASMCs (Fig. 3c, d(i, ii)) and TSMCs (Fig. 3d(iii)). Volume-rendered IC numbers also increased with distance from the base of the papilla (Supplementary Fig. 1ci–iii).

TSMCs and ASMCs

Figure 5ai illustrates the morphological differences between TSMCs (Fig. 5a(i) *cells within black box*) and ASMCs (Fig. 5a(i) *red box*) as revealed by standard electron microscopy. TSMCs were extremely elongated, darkly stained and compactly arranged in a layer adjacent to the urothelium. TSMCs contained densely packed parallel myofilaments and cisternae of granular endoplasmic reticulum clustered at the poles of their large oval-shaped nuclei. Mitochondria were randomly distributed throughout the cytoplasm. Three-dimensional reconstructions of TSMCs (Fig. 5a(ii) *dark green cells*) revealed that each cell was indeed elongated (Fig. 5b(i)) and mostly orientated in the circumferential direction (Fig. 5a(ii)).

ASMCs are located predominately on the serosal surface of the TSMC layer and occasionally between and within the TSMC bundles (Fig. 5a(i)). The nuclei of ASMCs were round and contained numerous clumps of nuclear chromatin [6]. ASMCs were irregular in shape due to the presence of long thin sarcoplasmic projections that formed close associations with neighbouring ASMCs and TSMCs (Fig. 5a(i)). In comparison to the TSMCs, ASMCs were loosely packed, the intervening space being occupied by a meshwork of collagen microfibrils (Fig. 5a(i)).

When volume rendered, the long thin projections of ASMCs observed in single EM sections (Fig. 5a(i)) were, in fact, continuous around a distinctive nuclear region (Fig. 5a(ii), b(ii) *pale green cells*). Thus, murine ASMCs were not 'stellate', nor 'spindle shaped' [7, 12, 20], but were irregular in shape with a nuclear region surrounded by a continuous cytoplasmic projection resembling the shape of a leaf (Fig. 5b(ii)). Figure 5c, d illustrates that individual TSMCs and ASMCs make close appositions with like cells (Fig. 5c(i, ii)) and each other (Fig. 5d(i, ii)). Examination of the three image stacks revealed that compared to the number of TSMCs, ASMCs were orientated mostly in the longitudinal direction and their relative number decreased with distance from the base of the papilla (Supplementary Fig. 1ci–iii).

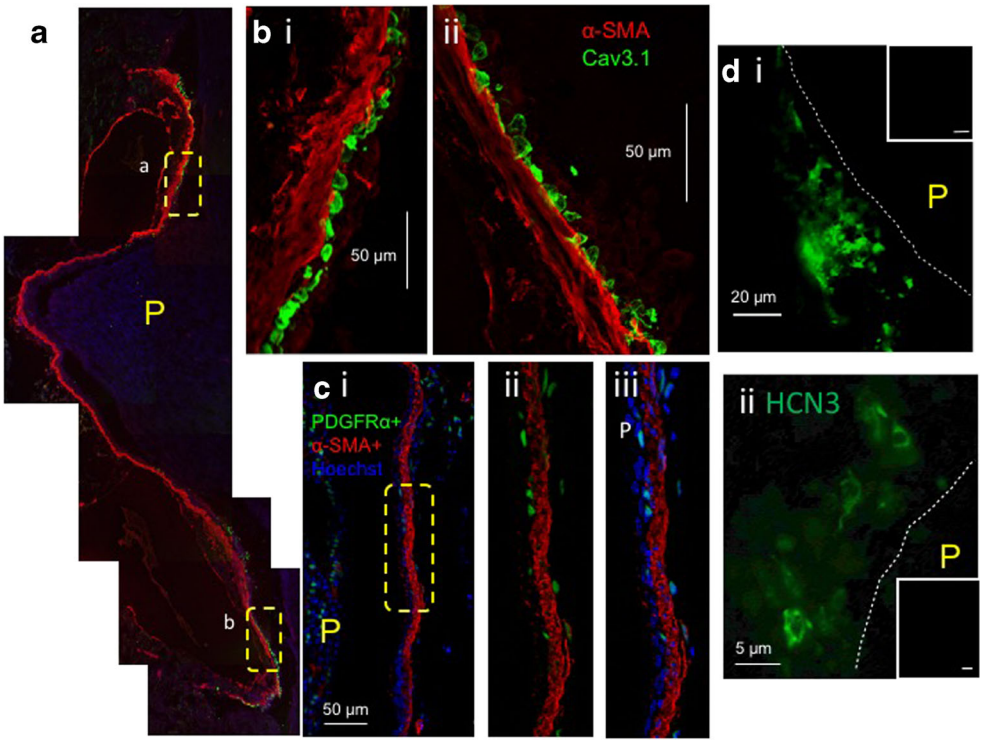

Fig. 4 Distribution of α-SMA and $Ca_V3.1$ immuno-reactivity in the mouse renal pelvis. **a** A collage of superimposed photomicrographs of a whole coronal section of mouse renal pelvis stained with antibodies for α-SMA (*red*) and $Ca_V3.1$ (*green*); nuclei were stained with Hoeschst (*blue*). **b**, *i–ii* Portions of renal pelvis indicated by boxes *a*, *b* in **a** are expanded to illustrate that the $Ca_V3.1$ immuno-reactive product was located within the sub-urothelial space. **c** PDGFRα(+) cells located in both the adventitia and the sub-urothelial space of the renal pelvis of a B6.129S4-$Pdgfr\alpha^{tm11(EGFP)sor}$/J mouse. **c**, *ii–iii* The box indicated in *i* was expanded to better illustrate that PDGFRα(+) cells were not immuno-positive for α-SMA and that they represented only a small proportion of the α-SMA(−) cells present. **d** Photomicrographs of whole mount of the bulb region (*i*) and septal attachment (*ii*) of the renal pelvis stained with antibodies for the HCN3 channel sub-unit. **d**, *i–ii Insets* are negative controls. *P* represents the papilla; the *dashed line* represents the luminal surface of the urothelium (colour figure online)

Blood vessels, macrophages and nerve bundles

Small renal arteries (RAs) and renal veins (RVs) were present in both the sub-urothelial and adventitial spaces, while larger vessels were located adjacent to the kidney parenchyma (Supplementary Fig. 1bi–iii). These blood vessels were readily volume rendered and displayed as solid structures or relatively transparent to reveal their red blood cells that could also be volume rendered.

Macrophages identified by the presence of electron dense bodies (endomes and lysosomes) were present within the renal pelvis wall (Supplementary Fig. 2ai–iii) and the BEC layer (Supplementary Fig. 2ci), as well as adjacent to and within the TSMC layer. Volume rendering of macrophages revealed that they were particularly long, extending considerable distances through the image stacks, very irregular in shape and made few contacts with any neighbouring cells (Supplementary Fig. 2aiv).

Nerve bundles were observed in all regions of the renal pelvis wall and often travelled great distances through the image stacks (Supplementary Fig. 2bi–iv). Volume rendering nerve bundles revealed that they made close appositions with small renal arteries and that they travelled within the TSMC bundles, as well as the BEC layer (Supplementary Fig. 2cii).

Effects of T-type and L-type Ca^{2+} channel blockers on renal pelvis contractility

As $Ca_V3.1$ channel immuno-reactivity has been located in the most proximal regions of the mouse renal pelvis (Fig. 4a, b), we have compared the inhibitory effects of two concentrations of Ni^{2+} (10 or 100 μM) that selectively block expressed $Ca_V3.2$ or reduce $Ca_V3.1$ channel sub-unit activity, respectively [19], with the inhibitory action of two other non-selective T-type Ca^{2+} channel blockers ML218 and mibefradil on both the contractile activity and Ca^{2+} signalling in the renal pelvis.

Figure 6a(i, ii), c(i, ii) illustrates typical decreases in renal pelvis diameter (downward deflections) plotted against time in the absence or presence of Ni^{2+} (10 μM), ML218 (1 μM) or nifedipine (1 μM), applied individually, or when two were applied together. These protocols revealed that Ni^{2+} (Fig. 6b(ii, iv)) and ML218 (Fig. 6d(ii, iv)) significantly reduced the frequency of contraction frequency, while

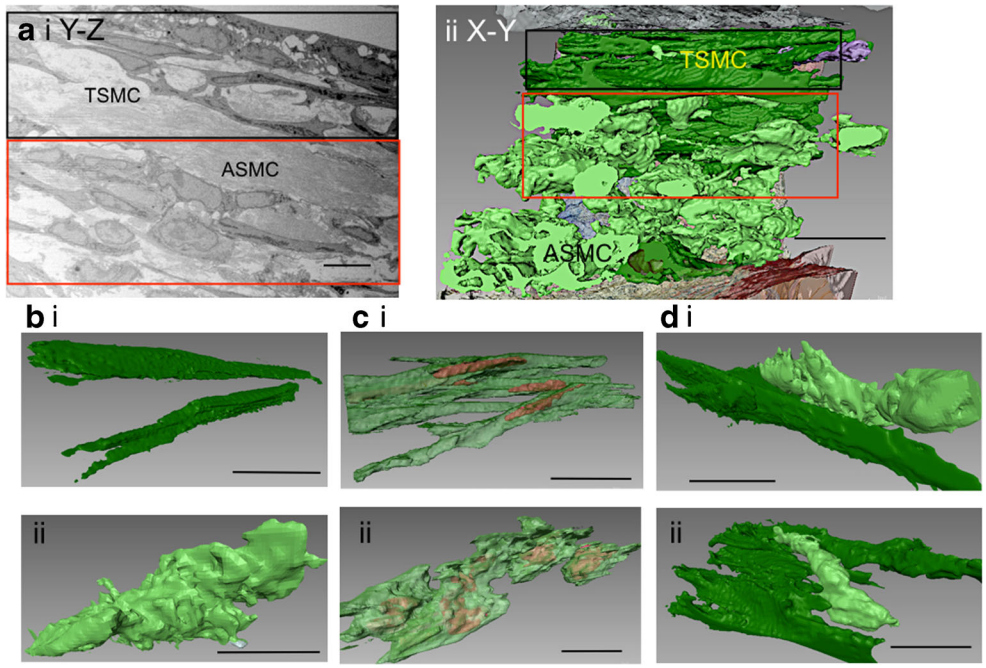

Fig. 5 Single cell reconstructions and close appositions of ASMCs and TSMCs. **a** Example of a single X-Y electron micrograph within the first image stack of ortho-slices illustrating the morphological difference between ASMCs (*i*, *red square*) and TSMCs (*i*, *black square*). *ii* Volume rendering the same region as *i* reveals the structure and association of the TSMCs (*dark green*) and ASMCs (*light green*) present. Typical examples of single or groups of TSMCs (**b**, *i*, **c**, *i*) and ASMCs (**b**, *ii*, **c**, *ii*) illustrating the differences in their shape and their close apposition with like cells. Cell walls have been projected as being solid (**b**, *i–ii*) or relatively transparent (**c**, *i–ii*) to reveal the shape and position of their volume-rendered nuclei. **d**, *i–ii* Examples of close appositions of TSMCs and ASMCs in the proximal renal pelvis. Calibration *bars* 0.5 μm (**a**), 0.3e^4 nm (**b**, *i*), 2e^5 nm (**b**, *ii*), 1e^4 nm (**c***i–ii*, **d**, *i*), 0.2e^4 nm (**d**, *ii*) (colour figure online)

nifedipine significantly reduced contraction amplitudes (Fig. 6b(i, iii), d(i, iii)). These results suggest that, as with gastrointestinal autorhythmicity, the presence of $Ca_V3.2$ channels may play an essential role in the propagation of excitation to electrically distant regions [36]. Mibefradil (10 μM) also significantly reduced control frequencies from 15.7 ± 2.1 to 11.9 ± 1.6 min^{-1} ($N = 9$ $p = 0.04$) without significantly reducing contraction amplitudes (−9.0 ± 7.2%, not significantly different from 0, $N = 9$, $p = 0.25$).

Effects of T-type Ca^{2+} channel blockers on TSMC Ca^{2+} transients

Regularly occurring Ca^{2+} transients were readily observed to sweep across the field of view within the TSMC layer of the renal pelvis when loaded with Fluo-4 (Fig. 7a) or Cal-520 (Fig. 7b–d). Ca^{2+} transients appeared simultaneously along the longitudinal axis of circumferentially orientated TSMCs and propagated distally into neighbouring cells. Long spindle-shaped regions of interest (ROIs) were drawn around two individual TSMCs 50–100 μm apart and their mean fluorescence measured and plotted against time as represented by the black and blue lines, respectively, in Fig. 7a–d. TSMC Ca^{2+} transients recorded with Cal-520 had a mean amplitude, ½ width and integral of 0.84 ± 0.07 F_t/F_0, 448.6 ± 21.5 ms and 440.6 ± 43.8 F_t/F_0 ms^{-1} ($N = 21$), respectively, and occurred at a frequency of 14.4 ± 1.4 min^{-1}.

Figure 7a(i, ii), c illustrates the effects of Ni^{2+} (10 and 100 μM) on the propagating Ca^{2+} transients in the TSMC layer. Ni^{2+} (10 μM) decreased the Ca^{2+} transient frequency by 60.4 ± 6.4% (Fig. 7e(i)) which was associated with a significant decrease in the basal Ca^{2+} of −0.07 ± 0.007 F_t/F_0 ($n = 12$ $N = 3$, $p = 0.000002$). The amplitude, ½ width and integral of the TSMC Ca^{2+} transients were not significantly altered by 10 μM Ni^{2+} (Fig. 7e(i)).

In contrast, the effects of 100 μM Ni^{2+} were more complex, resulting in a transient increase followed by a slow reduction in TSMC Ca^{2+} transient frequency (Fig. 7c), the transient excitation being associated with a transient rise in the TSMC basal Ca^{2+} of 0.19 ± 0.09 F_t/F_0 (significantly greater than 0, $n = 19$ $N = 5$ $p = 0.04$).

As with the contraction studies, TSMC Ca^{2+} transient amplitude, ½ width and integral were all significantly reduced in 1 μM nifedipine; their frequency was not significantly affected (Fig. 7e(ii)). The subsequent addition of nifedipine (1 μM) in the presence of Ni^{2+} (10 or 100 μM; Fig. 7a(ii), c) or Ni^{2+} (10 μM) added in the presence of nifedipine (1 μM; Fig. 7b) resulted in a complete blockade of TSMC Ca^{2+} transient firing.

Although ML218 (10 μM) did not significantly affect any parameters of TSMC Ca^{2+} transients (Fig. 7e(iii)), the

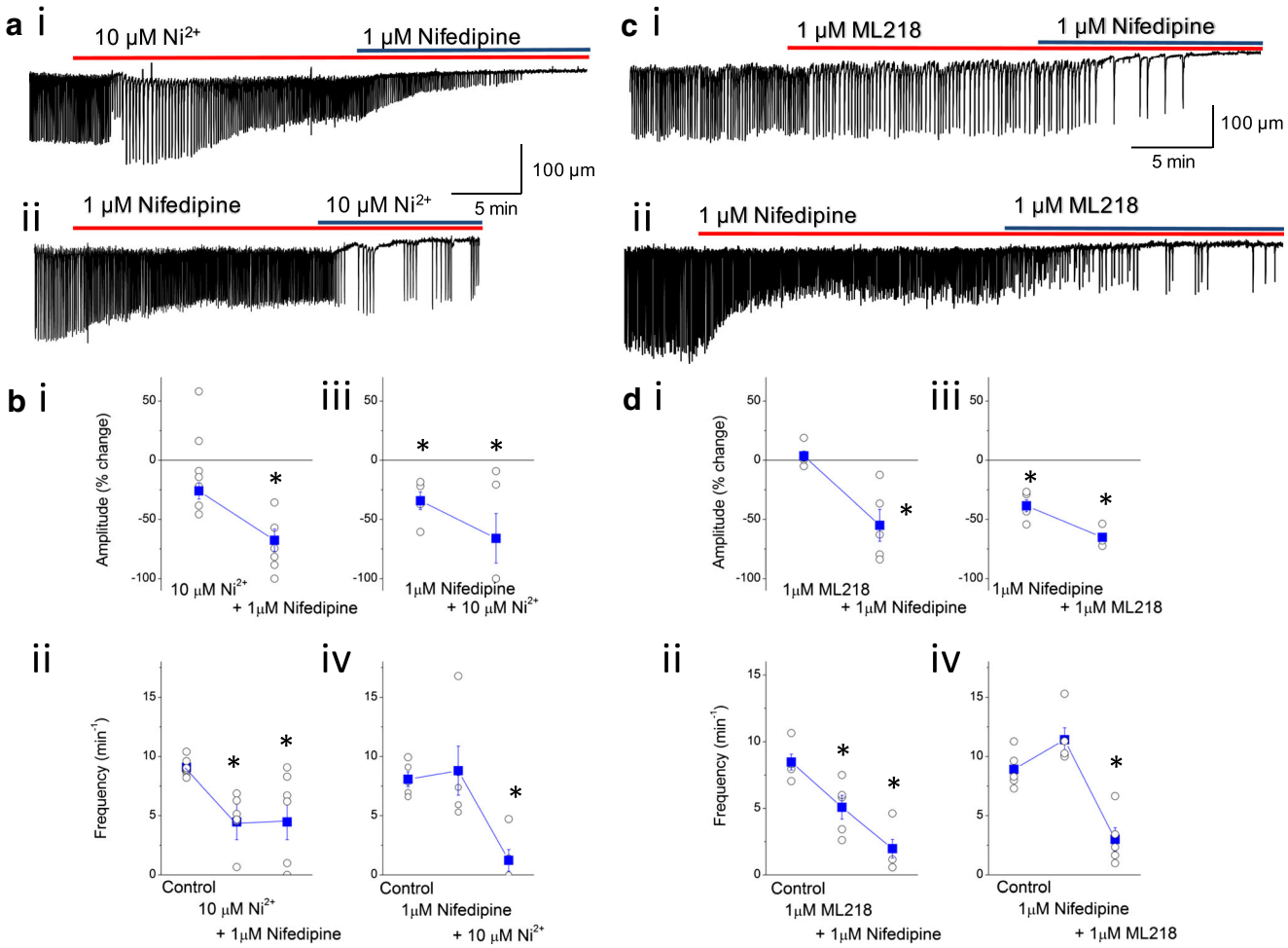

Fig. 6 Effects of T-type Ca^{2+} channel blockers on propagating contractions in the renal pelvis. Decreases in renal pelvis diameter (downward deflections) at one point on the renal pelvis were recorded with a video camera. Diamtrak software tracked and plotted these diameter changes against time in the absence or presence of Ni^{2+} (10 μM, **a**, *i*), ML218 (1 μM, **c**, *i*) or nifedipine (1 μM **a**, *ii*, **c**, *ii*). These protocols revealed that Ni^{2+} (**a**, *i*) and ML218 (**c**, *i*) significantly reduced the frequency of contraction frequency (**b**, *ii*, *iv*, **d**, *ii*, *iv*, $N = 5$) without affecting contraction amplitudes (**b**, *i*, **d**, *i*, $N = 5$), while nifedipine (**a**, *ii*, **c**, *ii*) significantly reduced contraction amplitudes (**b**, *iii*, **d**, *iii*, $N = 5$) without affecting contraction frequency (**b**, *iv*, **d**, *iv*)

subsequent addition of 1 μM nifedipine completely blocked TSMC Ca^{2+} activity (Fig. 7d).

IC and ASMC activity in the renal pelvis

Upon blockade of L-type Ca^{2+} channels with 1 μM nifedipine, Ca^{2+} transients in ICs and ASMCs were readily observed in the renal pelvis. IC Ca^{2+} transients were mostly recorded in the bulb region of the renal pelvis and in regions more distal, while ASMC Ca^{2+} transients were recorded both in the bulb region and in regions more proximal, within the finger-like attachments to the kidney parenchyma (Fig. 1a). ROIs for ASMCs were generally oval shaped, while IC ROIs were more rounded (Fig. 8a(i)).

IC Ca^{2+} transients ($N = 8$ $n = 17$) recorded with Cal-520 in the renal pelvis bathed in 1 μM nifedipine had a mean amplitude, ½ width and frequency significantly different from the equivalent parameters for ASMC Ca^{2+} transients ($N = 8$, $n = 25$) recorded in the same field of view (Table 1). However, small Ca^{2+} waves in the TSMC layer were also often seen to contaminate the IC and ASMC Ca^{2+} signals in 1 μM nifedipine-containing PSS. These residual TSMC Ca^{2+} waves were blocked upon the addition of Ni^{2+} (10–100 μM).

Figure 8a(ii–iv) illustrates typical spontaneous Ca^{2+} signals in three ICs (Fig. 8a(i, ii)) and two ASMCs (Fig. 8a(i, iii)) in a preparation bathed in PSS containing 1 μM nifedipine *plus* 100 μM Ni^{2+}. It can be seen that the ICs displayed spontaneous low-frequency, asynchronous Ca^{2+} transients that synchronized into a burst every 3–5 min. ASMCs displayed continuous higher-frequency spontaneous activity throughout the recording period, as well as an accelerated firing in synchrony with the bursting ICs.

A definitive distinction between 63 ICs ($N = 20$ Fig. 8b *black columns*) and 62 ASMCs ($N = 23$

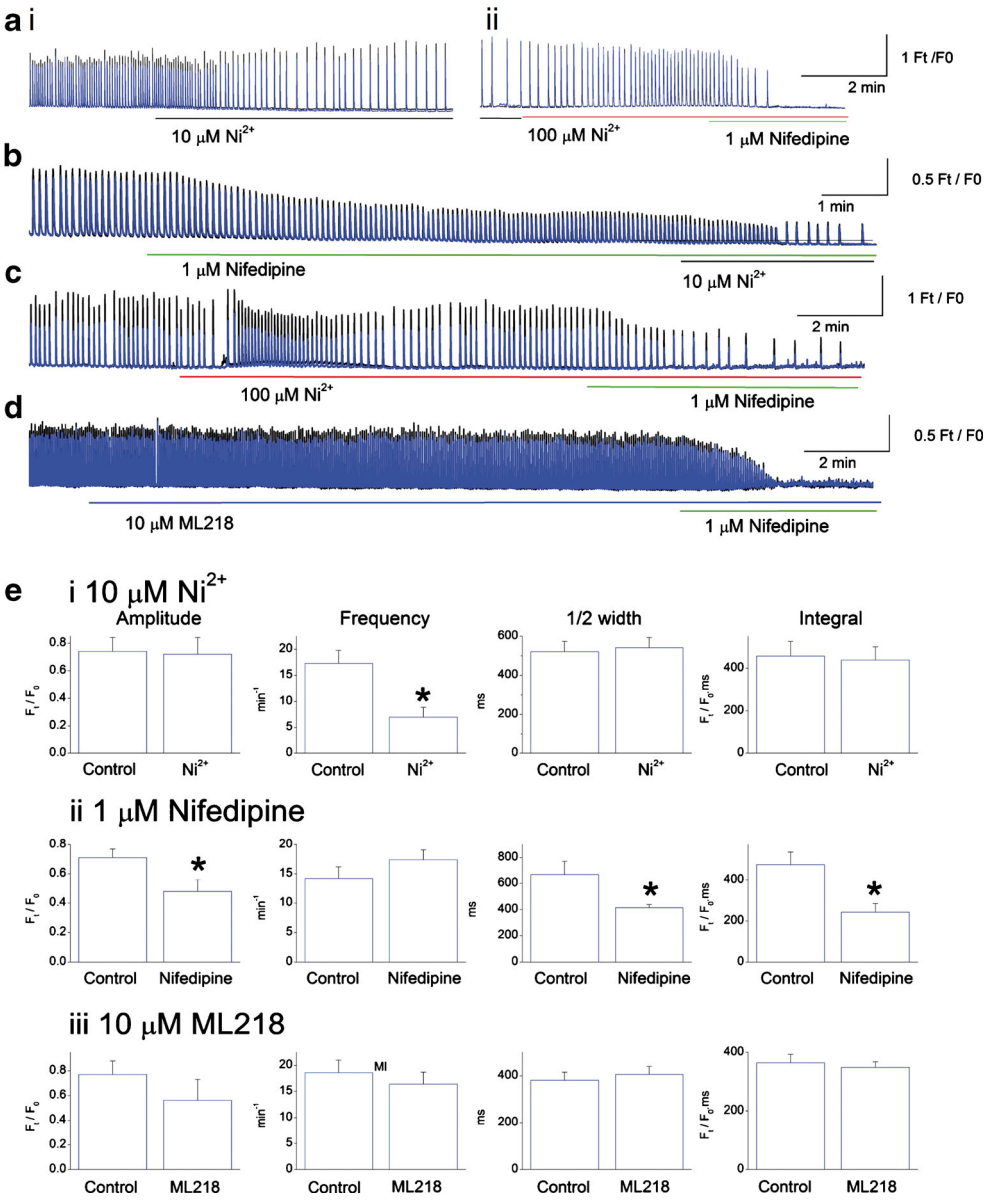

Fig. 7 Effects of T-type Ca^{2+} channel blockers on Ca^{2+} waves in the TSMC layer of the real pelvis. Ca^{2+} transients recorded in two TSMCs (*black* and *blue traces*) separated by 50–100 mm when loaded with Fluo-4 (**a**) or Cal-520 (**b**–**d**). TSMC Ca^{2+} transients were recorded in the absence or presence of 10 μM Ni^{2+} (**a**, *i*), 100 μM Ni^{2+} (**a**, *ii*, **c**), 1 μM nifedipine (**b**) or 10 μM ML218 (**d**). The subsequent addition of nifedipine (1 μM) in the presence of Ni^{2+} (10 or 100 μM, **a**, *ii*, **c**) or Ml218 (10 μM, **d**), or Ni^{2+} (10 μM) in the presence of nifedipine (1 μM, **b**) completely blocked TSMC Ca^{2+} transients. **e** Summary of the effects of 10 μM Ni^{2+} ($N = 7$, $^*p = 0.0002$, **e**, *i*), 1 μM nifedipine ($N = 7$, $^*p = 0.01$–0.03, **e**, *ii*) or 10 μM ML218 ($N = 5$, **e**, *iii*) on four measured parameters of TSMC Ca^{2+} transients (colour figure online)

Fig. 8b *blue columns*) bathed in PSS containing 1 μM nifedipine plus 100 μM Ni^{2+} was observed when their parameters measured *between* bursts were displayed as frequency distributions. It can be seen that ASMC parameters formed a single Gaussian distribution (Fig. 8b *red curves*, fitted by least squares) with their peak amplitude, ½ width, integral and frequency being summarized in Table 1. The frequency of these ASMC Ca^{2+} transients doubled *during* a burst of IC activity to a frequency similar to that in nifedipine alone (Table 1). Their basal Ca^{2+} also rose by 0.24 ± 0.05 F_t/F_0 (significantly different from 0, $p = 0.001$ $n = 20$). Mean ASMC amplitude, ½ width and integral *between* bursts were not significantly different from the equivalent parameters *during* a burst (Table 1).

In contrast, IC parameters were fitted by two Gaussian distributions with two peaks (Fig. 8b *green curves*) with their parameters summarized in Table 1. As it was not possible to ascribe ICs into a single normal distribution, IC activity was summed electrically (Fig. 8c(i–ii), d(i)) to examine their effects on neighbouring ASMCs. When the averaged F_t/F_0 (Fig. 8d(i)) for a number of ICs ($n = 3$–9) was plotted against the averaged F_t/F_0 (Fig. 8d(ii)) for three to seven ASMCs (Fig. 8c(i, iii)), a linear correlation was readily demonstrated (Fig. 8e *blue line*, $N = 5$).

Effects of HCN blocker ZD7288

The HCN channel blocker ZD7288 has been demonstrated to disrupt propagating peristaltic contractions in the mouse renal

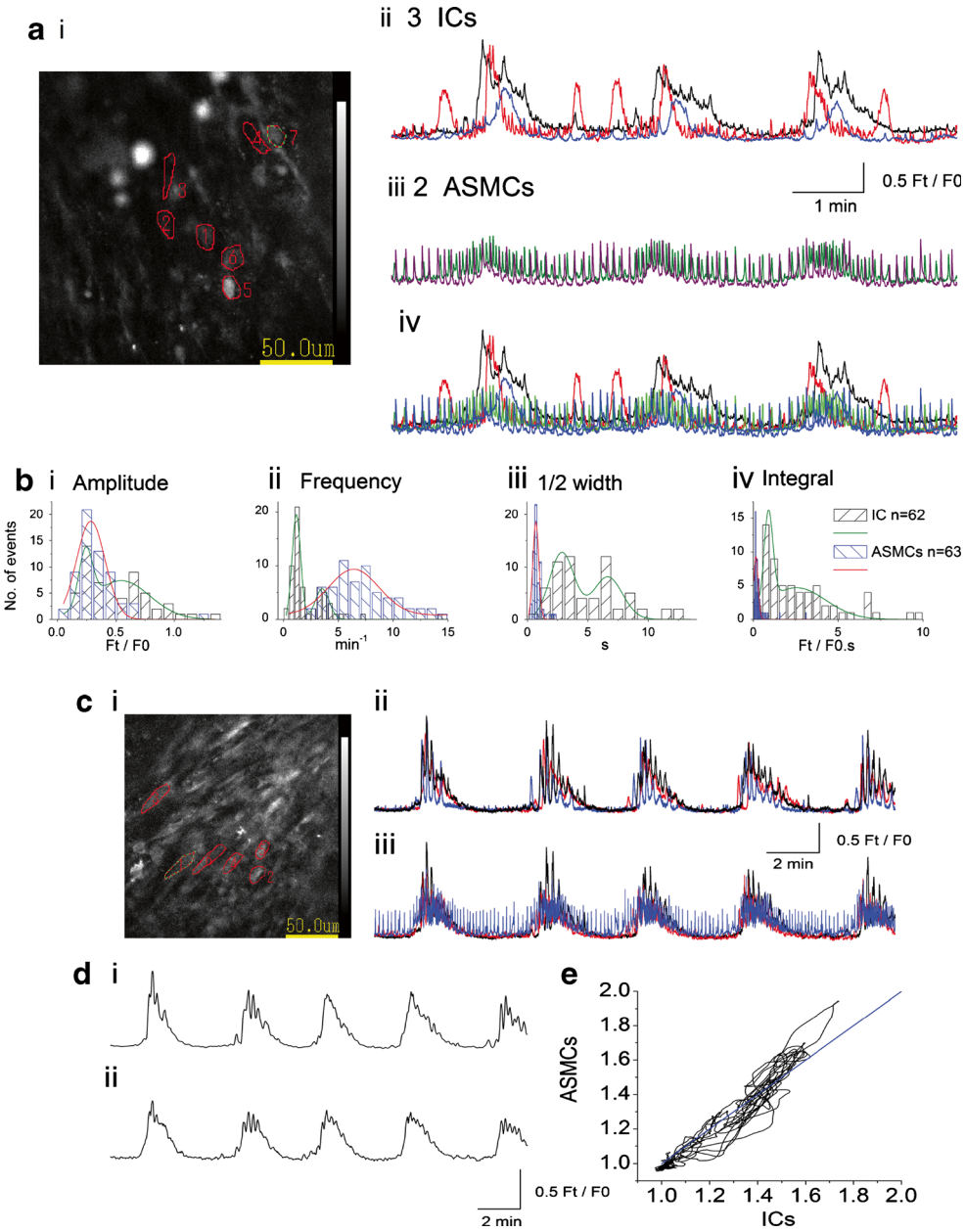

Fig. 8 Comparison of IC and ASMC Ca^{2+} transients in preparations of the renal pelvis. **a**, *i* typical field of view of cells displaying Ca^{2+} transients in a renal pelvis preparation, bathed in 1 μM nifedipine/100 μM Ni^{2+}-containing PSS. Ca^{2+} transient activity (F_t/F_0) in three ICs (**a**, *i* ROIs 1, 2, 5, **a**, *ii*) and two ASMCs (**a**, *i* ROIs 3, 4, **a**, *iii*) has been plotted against time separately (**a**, *ii–iii*) and together (**a**, *iv*). ICs displayed spontaneous low-frequency, asynchronous Ca^{2+} transients that synchronized into a burst every 3–5 min. Neighbouring ASMCs displayed higher-frequency spontaneous Ca^{2+} transients, as well as accelerated behaviour in synchrony with the bursting ICs. **b**, *i–iv* Frequency distributions of four measured parameters of 63 ICs (*blue columns*) and 62 ASMCs (*black columns*) recorded *between* bursts were fitted (by least squares) with one (**b**, *red* line) or two (**b**, *green line*) Gaussian distributions. Ca^{2+} transient activity (F_t/F_0) in three ICs (**c**, *i* ROIs 2, 4, 5, **c**, *ii*) and three ASMCs (**c**, *i* ROIs 1, 3, 6, **c**, *iii*) has been plotted against time separately (**c**, *ii–iii*, respectively) and after their activity has been averaged (**d**, *i* three ICs, **d**, *ii* three ASMCs). **e** Linear correlation (*blue line*) was evident when the averaged IC F_t/F_0 was plotted against the averaged ASMC F_t/F_0 (*black line*) (colour figure online)

pelvis, while HCN3(+) cells have been located at the site of excitation initiation within the renal pelvis papilla border [14, 15]. Thus, it has been suggested that these HCN3(+) cells play an important *voltage-dependent* pacemaker role in driving pyeloureteric peristalsis [14, 15].

In preparations bathed in 1 μM nifedipine plus 100 μM Ni^{2+}, Ca^{2+} transients in individual (Fig. 9a(i, ii)) and summed (Fig. 9a(iii), $n = 7$) ICs were rapidly inhibited in the presence of ZD7288 (30 μM for 10–20 min). The ability of these synchronized ICs to induce bursting behaviour in ASMCs within the same field of view was also inhibited (Fig. 9b(i, ii)).

ZD7288 (30 μM for 10–20 min) significantly decreased the frequency of ASMC Ca^{2+} transients ($N = 4$, $n = 12$) recorded in the quiescent periods between bursting IC activity (Fig. 9c(ii)), but had no significant effect on their mean amplitude, ½ width and integral (Fig. 9c(i, iii, iv)). The effects of ZD7288 were readily reversible after a 10–20-min washout.

In the present experiments, ZD7288 (10 and 20 μM for 10–30 min, $N = 6$) significantly decreased the frequency of the pelvic wall contractions (Fig. 9d(ii)), but did not significantly affect contraction amplitudes (Fig. 9d(i)).

Effects of carbenoxolone

The uncoupling of gap junctions with 18β-glycyrrhetinic acid has previously been demonstrated to rapidly block the

Table 1 Parameters of ASMCs and ICs in the mouse renal pelvis bathed in 1 μM nifedipine and 1 μM nifedipine plus 100 μM Ni^{2+}

	Amplitude F_t/F_0	Frequency min^{-1}	½ width ms	Integral F_t/F_0 ms^{-1}	*n*	*N*
1 μM nifedipine						
ASMCs	0.34 ± 0.04	13.7 ± 0.8	543.2 ± 32.1	204.7 ± 37.6	25	8
ICs	0.56 ± 0.09*	5.6 ± 0.9[#]	1237.9 ± 177.6[$]	1889.3 ± 1089.3	17	8
1 μM nifedipine plus 100 μM Ni^{2+}						
ASMCs						
Gaussian fit	0.28 ± 0.01	6.4 ± 0.3	700.4 ± 41.7	153.3 ± 12.9	62	20
ICs						
2 Gaussian fit	0.24 ± 0.02	1.18 ± 0.07	2865.6 ± 272.5	915 ± 139	63	20
	0.51 ± 0.07	3.5 ± 0.7	6647.7 ± 465.1	2552 ± 677		
ASMCs						
Between bursts	0.42 ± 0.05	7.4 ± 0.8	666.3 ± 94.3	313.8 ± 94.3	12	5
During bursts	0.38 ± 0.03	14.1 ± 1.1[e]	678.2 ± 90.1	278.6 ± 54.8	12	5

*p = 0.02

[#] p = 0.0000007

[$] p = 0.00004

[e] p = 0.00008

propagation of electrical and Ca^{2+} signals in the TSMC layer as well as slowly block ASMC Ca^{2+} transients [26]. In the present experiments, the effects of gap junction uncoupling with carbenoxolone on the ability of ICs to accelerate ASMC Ca^{2+} transient bursting was examined, as was the effects of carbenoxolone on renal pelvis contractility.

Figure 10 illustrates the effects of 50 μM carbenoxolone on the firing of Ca^{2+} transients in preparations bathed in 1 μM nifedipine plus 100 μM Ni^{2+}. Ca^{2+} signals in four ICs (Fig. 10(a), b(i)) and one ASMC (Fig. 10a, b(ii)) were displayed either separately or together (Fig. 10b(iii)). It can be seen that the bursting of IC Ca^{2+} transients was rapidly disrupted in carbenoxolone, as was the accelerated firing of the neighbouring ASMC. However, the asynchronous spontaneous activity in both cell types remained in the presence of carbenoxolone. Both phenomena were also rapidly restored upon carbenoxolone washout.

Carbenoxolone (10 and 30 μM, $N = 5$) decreased the amplitude (Fig.10c(i)) and frequency (Fig.10c(ii)) of contractions in the renal pelvis in a concentration manner.

Carbenoxolone has been implicated in modulating cyclooxygenase II activity [11, 39]. We have therefore examined the actions of the non-selective cyclooxygenase blocker indomethacin on the bursting behaviour of ICs and their modulation of ASMC Ca^{2+} transient discharge. In the presence of indomethacin (30 μM for 10–15 min), the amplitude and frequency of ASMC Ca^{2+} transients ($n = 15$, $N = 6$) recorded between bursts were significantly reduced by 37.8 ± 5.5% ($p = 0.0000007$) and 46.9 ± 6.1% ($p = 0.000002$), respectively, of control; their mean ½ width and integral were not significantly affected (all $p > 0.3$). The ICs in the two non-bursting preparations were also reduced in frequency and amplitude in the presence of indomethacin.

Discussion

From the earliest investigations into pyeloureteric peristalsis [10], it has been recognized that the origin of the peristaltic pressure waves in the renal pelvis was intrinsically 'myogenic', that the excitation originates in the proximal renal pelvis and travels distally towards the bladder. Our aim to identify and reconstruct the pacemaker cells within the mouse proximal renal pelvis to ascertain their gross architecture and associations necessitated image capture at relatively low SEM magnifications compared to previous observations [6–9, 12, 20]. However, these low-resolution electron micrographs allowed us to correlate the volume-rendered cell structures with those obtained immunohistologically or after loading with the Ca^{2+} fluorophores Fluo-4 or Cal-520.

TSMCs and ASMCs

There was remarkable concordance with the elongated shape and location of brightly fluorescent spindle-shaped α-SMA(+) TSMCs viewed in the bulb region of the renal pelvis wholemounts from eYFP-α-SMA(+) mice [17], with the cells that displayed Ca^{2+} waves in the absence of nifedipine [25] and the TSMCs volume rendered in the FIB SEM micrograph stacks. TMSCs mostly formed circumferentially orientated bundles of densely packed cells adjacent to the urothelium (Fig. 5a(ii)). Within the septa attachments proximal of the bulb region, TSMCsdecrease in number and are mostly absent as the renal pelvis approaches the papilla base [17, 20, 27]. In the septal attachments, lightly fluorescent α-SMA(+) ASMCs are loosely arranged in a basket weave arrangement while in the bulb region

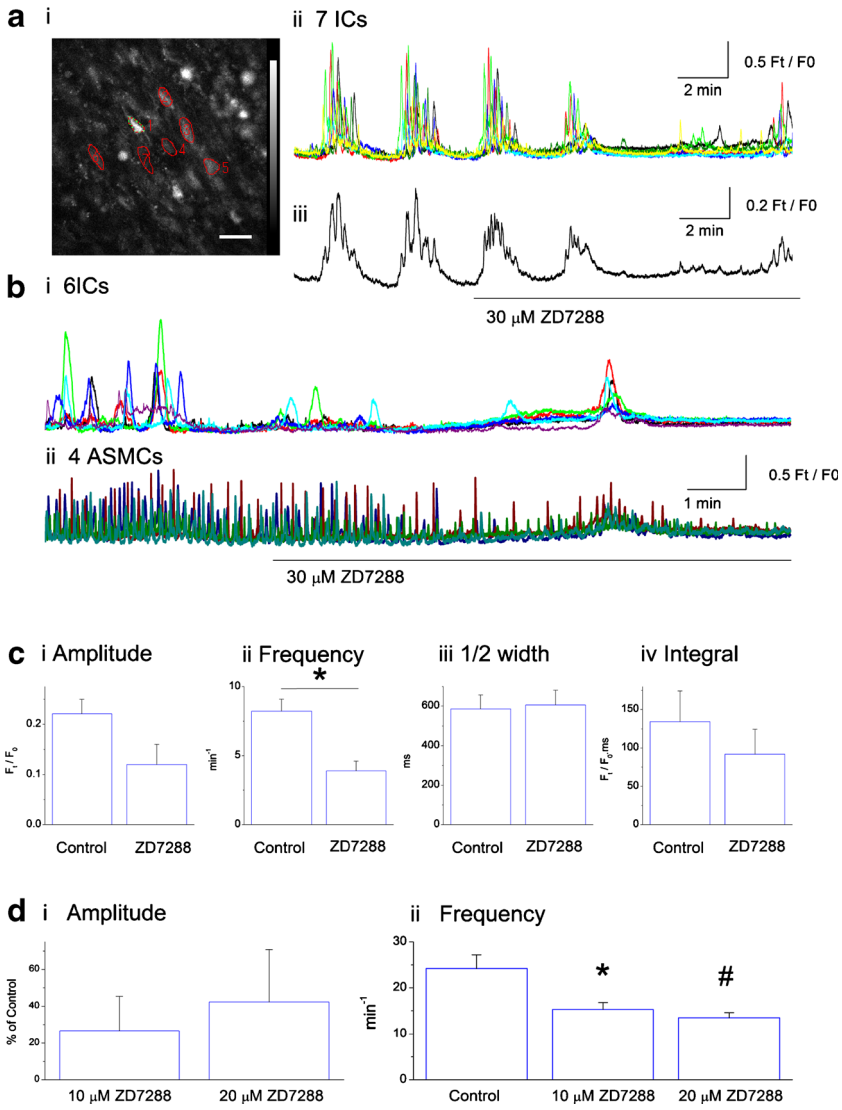

Fig. 9 Effects of the HCN channel blocker ZD7288 on Ca^{2+} transients in TSMCs and ASMCs. In preparations bathed in 1 μM nifedipine plus 100 μM Ni^{2+} PSS and imaged with Cal-520, spontaneous Ca^{2+} transients in six to seven ICs displayed individually (**a**, *i*, **b**, *i*) or after averaging (**a**, *iii*) were rapidly inhibited in the presence of ZD7288 (30 μM for 10 min), as was their excitatory action on neighbouring ASMCs (**b**)*ii*. *Scale bar* 50 μm. **c** Summary of the effects of 30 μM ZD7288 ($N = 4$, $n = 12$, $*p = 0.002$) on the four measured parameters of ASMC Ca^{2+} transients. **d** Effects of ZD7288 (10 and 20 μM, $N = 6$) on the amplitude (**d**, *i*) and frequency (**d**, *ii*) of renal pelvis contractions. $*p = 0.03$, $\#p = 0.04$

they are mostly longitudinally arranged in a focal plane adventitial to the TSMC layer (Fig. 5a(ii)) [17], in the same region as ASMCs identified using standard electron microscopy (Fig. 5a(i)) [7, 8, 12, 20, 27].

In single electron microscopic sections, ASMCs appear as having a rounded nuclear region with radiating thin projections and have previously been interpreted as being stellate or spindle shaped (Fig. 5a(i)) [7, 12, 20, 27]. The present FIB SEM experiments have established that these ASMC projections were thin but continuous, so that they resemble the rim of an irregular saucer or leaf (Fig. 5b(ii)). Importantly, these volume-rendered ASMCs are in the same morphological space as the ASMCs displaying high-frequency spontaneous Ca^{2+} transients in contraction-arrested preparations. The present experiments have also established that volume-rendered ASMCs and the cells firing high-frequency Ca^{2+} transients both become more sparsely distributed with distance from the papilla base (Supplementary Fig. 1ci–iii) [7, 8, 12, 20].

Sub-urothelial and serosal ICs

Volume-rendered ICs in the renal pelvis were found in both the adventitia and sub-urothelial space [27] and make close appositions with both ASMCs and TSMCs. ICs appear to represent a mixed population of cells that has yet to be fully characterized. One set of α-SMA(−) ICs are immuno-positive for Ano1 Cl^- and $K_V7.5$ channel proteins (Fig. 3b(i–ii)) and are likely to be the same as the freshly isolated ICs that display spontaneous transient niflumic acid-sensitive Cl^- currents, as well as voltage-dependent K^+ current sensitive to the $K_V7.x$ channel blocker XE911 [17]. Similarly, a population of cells, which may [29, 30, 38] or may not [20] be immuno-reactive to antibodies raised against the *c-Kit* proto-oncogene, the

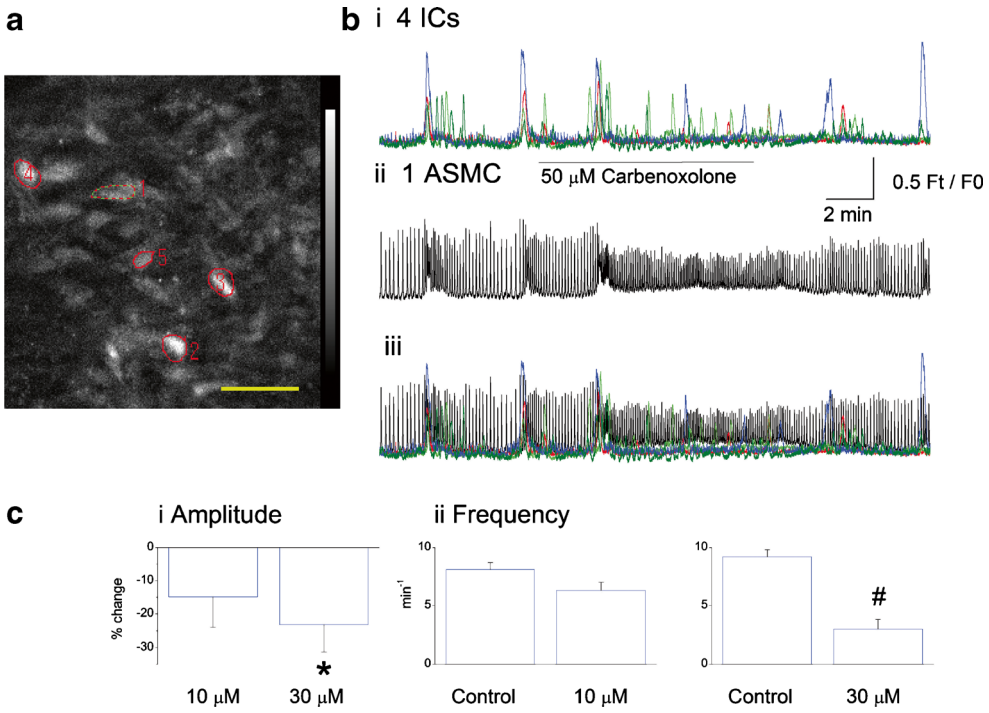

Fig. 10 Effects of blocking cell coupling with carbenoxolone on Ca^{2+} transient discharge in ICs and ASMCs. Ca^{2+} transient activity (Ft/F_0) in four ICs (**a** ROIs 2–5, **b**, *i*) and one ASMC (**a** ROI 1, **b**, *ii*) was plotted either separately (**b**, *i–ii*) or together (**b**, *iii*) against time. It can be seen that the bursting of IC Ca^{2+} transients and the excitation of the ASMC was rapidly disrupted in 50 μM carboxelone. However, their spontaneous activity remained in the presence of carboxelone. *Scale bar* 50 μm. **c** Effects of carbenoxolone (10 and 30 μM, $N = 6$) on the amplitude (**c**, *i*) and frequency (**c**, *ii*) of the pelvic wall contractions. $^*p = 0.03$, $\#p = 0.001$

selective marker of gastrointestinal interstitial cells of Cajal (ICC), has also been reported in the renal pelvis. These Kit(+) cells appear at the same time as the establishment of uni-directional peristalsis in the ureter [4, 5], as well as being reduced in number during cogential ureteropelvic junction obstruction [38], or in theobstructive megaureter [1, 2, 18], leading to the suggestion that they also play a critical role in promoting pyeloureteric peristalsis.

$HCN3^+$ ICs

HCN3(+) cells have been reported to be 'integrated' within the smooth muscle layer of the proximal region of the uni-calyceal mouse renal pelvis [14, 15] and the minor calyces of porcine and human multi-calyceal kidney [16]. These HCN3(+) cells have been co-located with $Ca_V3.1$ channel immuno-reactivity in the mouse renal pelvis [14] and $Ca_V3.2$ channel immuno-reactivity in porcine and human multi-calyceal kidneys [16]. There appears to be some confusion as to whether HCN3 staining co-locates with α-SMA immuno-reactivity in the renal pelvis. In the present experiments, $Ca_V3.1$(+) cells did not co-locate with α-SMA immuno-reactivity and clearly lay only in the sub-urothelial space of the proximal renal pelvis (Fig. 4a, b). However, Hurtado et al. [15] reported that $HCN3^+$ $Ca_V3.1$(+) cells also express α-SMA immuno-reactivity and, although not stated, appear to lie within the sub-urothelial space (Fig. 5B–D of [15]). In contrast, HCN3(+) cells in the minor calyces of the porcine kidney express both α-SMA and $Ca_V3.2$ immuno-reactivity, while HCN3(+) and $Ca_V3.2$(+) cells in the human minor calyces do not appear to co-locate with α-SMA immuno-reactivity [16].

In spite of our pharmacological evidence of the effects of low concentrations of Ni^{2+} and therefore the likely blockade of $Ca_V3.2$ channels (Ni^{2+} IC_{50}, 5 μM) [19], on TSMC Ca^{2+} waves and contraction in the mouse renal pelvis, we and others [14, 15] have failed to demonstrate the presence of $Ca_V3.2$ channel immuno-reactivity. Thus, there appears to be some species-dependent selectivity issues using presently available antibodies.

Future identification of IC sub-populations

Further investigations, confirming putatively selective markers of mouse ASMCs (low α-SMA(+)), TSMCs (intensely α-SMA(+), Ano1(+) and $K_V7.4$(+)), BECs ($K_V7.5$(+) and $K_V7.4$(+)), fibroblast-like ICs ($K_V7.5$(+), $K_V7.4$(+) and Ano1(+)) [17], HCN3(+) and $Ca_V3.1$(+) cells [14], PDGFRα(+) cells and sub-urothelial $Ca_V3.1$(+) ICs (Fig. 4) need to be undertaken using mRNA and protein level analysis after cell sorting. Combining other cell-specific markers for Kit, cyclooxygenase I and II, myosin heavy chain, ryanodine receptors, urothelium, etc., may well lead to the development of cell-specific reporter mouse strains allowing the creation of specific knock-out/knock-in or genetically encoded Ca^{2+} indicator models for the unequivocal identification and study of sub-urothelial and adventitial ICs, as well as distinguishing between TSMCs and ASMCs.

Ca^{2+} signalling in ASMCs

An extensive examination of the temporal properties of the Ca^{2+} transients in ASMCs and ICs in preparations bathed in 1 μM nifedipine plus 100 μM Ni^2 demonstrated they were significantly different. ASMC Ca^{2+} transient parameters were described by single Gaussian distributions suggesting that ASMCs represented a single population of cells firing at a frequency of 6–13 min^{-1}. ASMCs are little affected upon the addition of ryanodine [26] or tetracaine (unpublished data, H Hashitani and RJ Lang) and reduced or blocked by cyclopiazonic acid, 2-aminoethooxy-diphenylboarate, neomycin or U73122 [26], suggesting that ASMC Ca^{2+} signalling arises predominately from the uptake and release of Ca^{2+} from inositol triphosphate (IP_3)-dependent Ca^{2+} stores [26].

The decrease in frequency (14 to 7 min^{-1}) but not blockade of ASMC Ca^{2+} transient firing when Ni^{2+} (100 μM Ni^{2+}) was added to preparations exposed to only nifedipine suggests that voltage-dependent Ca^{2+} entry through T-type Ca^{2+} channels enhances this IP_3 receptor-mediated Ca^{2+} release via mechanisms of Ca^{2+}-induced release of Ca^{2+} [26, 31]. The immunohistochemical evidence (Fig. 4a, b) and the IC modulation of ASMC activity observed in preparations bathed in 1 μM nifedipine plus 100 μM Ni^{2+}, which would only reduce $Ca_V3.1$ channel openings, suggest that these T-type channels are located on neighbouring ICs.

Ca^{2+} signalling in ICs

In the present experiments, the use of the Ca^{2+} fluorophore Cal-520 with its increased penetration and fluorescence has allowed a greater loading and recording from ICs than previously reported [25]. The parameters of IC Ca^{2+} transients were best described by two Gaussian distributions, firing at frequencies of 1.1 and 3.5 min^{-1} (Fig. 8b). IC Ca^{2+} transients also displayed synchronized bursting behaviour, occurring at a frequency of once every 3–5 min, even when cells were separated by 50–200 μm (Figs. 8–10). As it was not possible to ascribe ICs into a single normal distribution, IC activity was summed electrically to examine their effects on neighbouring ASMCs. When a number of ICs (n = 3–9) were summed together, the averaged Ft/F_0 correlated in time with the change in baseline and the accelerated response of ASMCs within the same field of view (Fig. 8e). A small increase in TSMC basal Ca^{2+} was also sometimes observed during these bursts of IC Ca^{2+} transients.

To date, neither a $Ca_V3.1$ nor an HCN current have been recorded in single α-SMA(−) ICs of the mouse renal pelvis [17], even though robust HCN and 'T-type' Ca^{2+} currents are readily recorded in cultured mouse dorsal root ganglia under the same laboratory conditions (RJ Lang, unpublished data). Given the relatively high resting membrane resistance of single ICs (5.7 GΩ) [17], an HCN3 channel current, no matter how small, could well make an essential contribution to the IC resting membrane potential or the membrane depolarization that shifts the membrane potential back towards threshold after the firing of an action potential [3, 20]. Consistent with such a contribution is the co-location of HCN3 and $Ca_V3.1$ channel immuno-reactivity in α-SMA(−) ICs [14, 15] and the present results that IC Ca^{2+} transients were abolished upon the addition of ZD7288 in the presence of Ni^{2+} and nifedipine (Fig. 9).

Given the relatively high Ni^{2+} IC_{50} (350 μM) for $Ca_V3.1$ channels [19], 100 μM Ni^{2+} would only partially block these channels in the renal pelvis. Blockade of HCN3 currents may well lead to IC hyperpolarization to potentials negative of the opening threshold of any residual $Ca_V3.1$ channels and reduce Ca^{2+} entry. The effects of such a reduction of T-type channel Ca^{2+} entry on IC Ca^{2+} transient frequency was also evident when Ni^{2+} (100 μM) was added in the presence of nifedipine. These data suggest that voltage-dependent Ca^{2+} entry through $Ca_V3.1$ Ca^{2+} channels enhances Ca^{2+} release from ryanodine-sensitive internal Ca^{2+} stores which contributes to IC Ca^{2+} signalling [26].

IC modulation of ASMCs

The change in baseline and the acceleration of ASMC Ca^{2+} transients associated with synchronized bursting of IC Ca^{2+} transients were blocked by the gap junction inhibitor carbenoxolone (Fig. 10). However, the asynchronous firing of both cell types remained, suggesting that ICs were electrically coupled to other ICs, as well as ASMCs in the same field of view. In the presence of both L-type and T-type Ca^{2+} channel blockers, the spread of depolarization between neighbouring cells is likely to be intercellular and slowly voltage dependent, arising from the Ca^{2+}-activated membrane currents generated by the spontaneous IC Ca^{2+} transients [17]. In the absence of Ca^{2+} channel blockade, these spontaneous membrane depolarizations in ICs would be more effective at accelerating ASMC STD summation to trigger action potentials in neighbouring TSMCs.

The comparison of the effects of carbenoxolone and indomethacin on IC and ASMC Ca^{2+} activity establishes that carbenoxolone was not acting as a cyclooxygenase inhibitor [11, 39] and that prostaglandin release does more than just maintain cell-to-cell coupling [23]. The abolition of IC Ca^{2+} transients, ASMC activity and pyeloureteric peristalsis [22, 37] upon cyclooxygenase inhibition suggests that their spontaneous activity is being fuelled by an autocrine/paracrine mechanism and that the paracrine agent may well be a prostanoid. In the upper urinary tract, applied prostaglandin $(PG)F_{2\alpha}$ is generally excitatory, PGE_1 inhibitory, while PGE_2 has a mixed excitatory and inhibitory action [22]. We

envisage that locally released prostaglandins binding to G protein-coupled receptors on both ICs and ASMCs contribute to the IP_3 formation that drives their Ca^{2+} cycling [21].

In summary, the present experiments have established that adventitial and sub-urothelial ICs are long, ribbon-shaped cells that provide a low-frequency modulation of leaf-shaped ASMCs via an intercellular means. The close apposition of ICs with neighbouring ASMCs and TSMCs suggests that HCN3(+) and $Ca_V3.1$(+) ICs generate a direct slow intercellular voltage-dependent modulation of pyeloureteric excitability. Thus, ICs do not represent the primary pacemaker driving pyeloureteric peristalsis; rather, they may act as an accelerator of the ASMC-derived pacemaker drive. However, impaired urine flow arising from a functional obstruction often leads to the development of back pressure-induced atrophy of the most proximal regions of the renal pelvis and presumably a reduction of the proximal ASMC pacemaking. The present experiments have demonstrated that ICs can directly modulate ASMC activity. It has yet to be established whether ICs within the distal renal pelvis in mildly hydronephrotic kidneys can directly modulate TSMC excitability to maintain a rudimentary pyeloureteric peristalsis in the absence of a proximal ASMC pacemaker drive.

Acknowledgements The work was supported by Grant-in-Aid for Scientific Research (No. 26670705) from the Japan Society for Promotion of the Science (JSPS) to H.H. The authors acknowledge the use of the imaging facilities within the Multi-modal Australian ScienceS Imaging and Visualization Environment (MASSIVE) at the Monash University node of the National Imaging Facility.

Compliance with ethical standards

Funding The work was supported by Grant-in-Aid for Scientific Research (No. 26670705) from the Japan Society for Promotion of the Science (JSPS) to H.H.

Conflict of interest The authors declare that they have no conflict of interest.

Ethical approval All procedures performed in studies involving animals were in accordance with the ethical standards of the institutions at which the studies were conducted.

Informed consent Informed consent was obtained from all individual participants included in the study.

References

1. Arena E, Nicotina PA, Arena S, Romeo C, Zuccarello B, Romeo G (2007a) Interstitial cells of Cajal network in primary obstructive megaureter. Pediatr Med Chir 29:28–31
2. Arena F, Nicotina PA, Arena S, Romeo C, Zuccarello B, Romeo G (2007b) C-kit positive interstitial cells of Cajal network in primary obstructive megaureter. Minerva Pediatr 59:7–11
3. Biel M, Wahl-Schott C, Michalakis S, Zong X (2009) Hyperpolarization-activated cation channels: from genes to function. Physiol Rev 89:847–885
4. Cain JE, Islam E, Haxho F, Blake J, Rosenblum ND (2011) Gli3 repressor controls functional development of the mouse ureter. J Clin Invest 121:1199–1206
5. David SG, Cebrian C, Vaughan ED, Herzlinger D (2005) C-Kit and ureteral peristalsis. J Urol 173:292–295
6. Dixon JS, Gosling JA (1970a) Electron microscopic observations on the renal caliceal wall in the rat. Zeitschrift Fur Zellforschung Und Mikroskopische Anatomie 103:328–340
7. Dixon JS, Gosling JA (1970b) Fine structural observations on the attachment of the calix to the renal parenchyma in the rat. J Anatomy 106:181–182
8. Dixon JS, Gosling JA (1973) The fine structure of pacemaker cells in the pig renal calices. Anat Rec 175:139–153
9. Dixon JS, Gosling JA (1982) The musculature of the human renal calices, pelvis and upper ureter. J Anatomy 135:129–137
10. Englemann TW (1869) Zur Physiologie Des Ureter. Pflugers Archiv Eur J Physiol 2:243–293
11. Ergang P, Leden P, Bryndova J, Zbankova S, Miksik I, Kment M, Pacha J (2008) Glucocorticoid availability in colonic inflammation of rat. Dig Dis Sci 53:2160–2167
12. Gosling JA, Dixon JS (1974) Species variation in the location of upper urinary tract pacemaker cells. Investig Urol 11:418–423
13. Hashitani H, Lang RJ, Mitsui R, Mabuchi Y, Suzuki H (2009) Distinct effects of Cgrp on typical and atypical smooth muscle cells involved in generating spontaneous contractions in the mouse renal pelvis. Br J Pharmacol 158:2030–2045
14. Hurtado R, Smith CS (2016) Hyperpolarization-activated cation and T-type calcium ion channel expression in porcine and human renal pacemaker tissues. J Anat 228:812–825
15. Hurtado R, Bub G, Herzlinger D (2010) The pelvis-kidney junction contains Hcn3, a hyperpolarization-activated cation channel that triggers ureter peristalsis. Kidney Int 77:500–508
16. Hurtado R, Bub G, Herzlinger D (2014) A molecular signature of tissues with pacemaker activity in the heart and upper urinary tract involves coexpressed hyperpolarization-activated cation and T-type Ca^{2+} channels. FASEB J 28:730–739
17. Iqbal J, Tonta MA, Mitsui R, Li Q, Kett M, Li J, Parkington HC, Hashitani H, Lang RJ (2012) Potassium and Ano1/Tmem16a chloride channel profiles distinguish atypical and typical smooth muscle cells from interstitial cells in the mouse renal pelvis. Br J Pharmacol 165:2389–2408
18. Kang H, Park J, Jeong S, Kim J, Moon H, Perez-Reyes E, Lee J (2006) A molecular determinant of nickel inhibition in Cav3.2 T-type calcium channels. J Biol Chem 281:4823–4830
19. Kang H, Lee H, Jin M, Jeong H, Han S (2009) Decreased interstitial cells of Cajal-like cells, possible cause of congenital refluxing Megaureters: histopathologic differences in refluxing and obstructive Megaureters. Urology 74:318–323
20. Klemm M, Exintaris B, Lang R (1999) Identification of the cells underlying pacemaker activity in the guinea-pig upper urinary tract. J Physiol 519:867–884
21. Lang R (2010) Role of hyperpolarization-activated cation channels in pyeloureteric peristalsis. Kidney Int 77:483–485
22. Lang RJ, Klemm MF (2005) Interstitial cell of Cajal-like cells in the upper urinary tract. J Cell Mol Med 9:543–556
23. Lang R, Exintaris B, Teele M, Harvey J, Klemm M (1998) Electrical basis of peristalsis in the mammalian upper urinary tract (review). Clin Exp Pharmacol Physiol 25:310–321
24. Lang RJ, Takano H, Davidson ME, Suzuki H, Klemm MF (2001) Characterization of the spontaneous electrical and contractile activity of smooth muscle cells in the rat upper urinary tract. J Urol 166: 329–334

25. Lang R, Davidson M, Exintaris B (2002) Pyeloureteral motility and ureteral peristalsis: essential role of sensory nerves and endogenous prostaglandins. Exp Physiol 87:129–146
26. Lang R, Hashitani H, Tonta M, Parkington H, Suzuki H (2007a) Spontaneous electrical and Ca^{2+} signals in typical and atypical smooth muscle cells and interstitial cell of Cajal-like cells of mouse renal pelvis. J Physiol 583:1049–1068
27. Lang RJ, Hashitani H, Tonta MA, Suzuki H, Parkington HC (2007b) Role of Ca^{2+} entry and Ca^{2+} stores in atypical smooth muscle cell autorhythmicity in the mouse renal pelvis. Br J Pharmacol 152:1248–1259
28. Lang R, Hashitani H, Tonta M, Bourke J, Parkington H, Suzuki H (2010) Spontaneous electrical and Ca^{2+} signals in the mouse renal pelvis that drive pyeloureteric peristalsis. Clin Exp Pharmacol Physiol 37:509–515
29. Kj P, Gw H, Lee H, Spencer N, Ward S, Smith T, Sanders K (2006) Spatial and temporal mapping of pacemaker activity in interstitial cells of Cajal in mouse ileum in situ. Am J Physiol-Cell Physiol 290:C1411–C1427
30. Metzger R, Schuster T, Till H, Stehr M, Franke FE, Dietz HG (2004) Cajal-like cells in the human upper urinary tract. J Urol 172:769–772
31. Metzger R, Schuster T, Till H, Franke FE, Dietz HG (2005) Cajal-like cells in the upper urinary tract: comparative study in various species. Pediatr Surg Int 21:169–174
32. Miyakawa T, Mizushima A, Hirose K, Yamazawa T, Bezprozvanny I, Kurosaki T, Iino M (2001) Ca^{2+}-sensor region of Ip3 receptor controls intracellular Ca^{2+} signaling. EMBO J 20:1674–1680
33. Nguyen MJ, Angkawaijawa S, Hashitani H, Lang RJ (2013) Nicotinic receptor activation on primary sensory afferents modulates autorhythmicity in the mouse renal pelvis. Brit J Pharmacol 170:1221–1232
34. Nguyen MJ, Higashi R, Ohta K, Nakamura KI, Hashitani H, Lang RJ (2015) Autonomic and sensory nerve modulation of peristalsis in the upper urinary tract. Auton Neurosci. doi:10.1016/J.Autneu.2015.07.425
35. Nguyen MJ, Hashitani H, Lang RJ (2016) Angiotensin receptor-1a knockout leads to hydronephrosis not associated with a loss of pyeloureteric peristalsis in the mouse renal pelvis. Clin Exp Pharmacol Physiol 43:535–542
36. Ohta K, Sadayama S, Togo A, Higashi R, Tanoue R, Nakamura K (2012) Beam deceleration for block-face scanning electron microscopy of embedded biological tissue. Micron 43:612–620
37. Santicioli P, Maggi CA (1998) Myogenic and neurogenic factors in the control of pyeloureteral motility and ureteral peristalsis. Pharmacol Rev 50:683–722
38. Solari V, Piotrowska AP, Puri P (2003) Altered expression of interstitial cells of Cajal in congenital ureteropelvic junction obstruction. J Urol 170:2420–2422
39. Thakur P, Nehru B (2015) Inhibition of neuroinflammation and mitochondrial dysfunctions by carbenoxolone in the rotenone model of Parkinson's disease. Mol Neurobiol 51:209–219
40. Tsuchida S, Suzuki T (1992) Pacemaker activity of the pelvicalyceal border recorded by an intracellular glass microelectrode. Urol Int 48:121–124